frontiers | Frontiers in Physics

TYPE Original Research
PUBLISHED 10 January 2023
DOI 10.3389/fphy.2022.1118917

OPEN ACCESS

EDITED BY
Wenjun Liu,
Beijing University of Posts and Telecommunications (BUPT), China

REVIEWED BY
Xinbing Wang,
Huazhong University of Science and Technology, China
Zhenxu Bai,
Hebei University of Technology, China

*CORRESPONDENCE
Hao Li,
hli@simtech.a-star.edu.sg

SPECIALTY SECTION
This article was submitted to Optics and Photonics, a section of the journal Frontiers in Physics

RECEIVED 08 December 2022
ACCEPTED 23 December 2022
PUBLISHED 10 January 2023

CITATION
Ran Q, Short JS, Wang QJ and Li H (2023), A 206-nm all-solid-state deep-ultraviolet laser with 291 MW peak power. *Front. Phys.* 10:1118917. doi: 10.3389/fphy.2022.1118917

A 206-nm all-solid-state deep-ultraviolet laser with 291 MW peak power

Qiandong Ran[1,2], Joel Stephen Short[3], Qi Jie Wang[2] and Hao Li[1]*

[1]Advanced Imaging and Machine-Vision Group, Singapore Institute of Manufacturing Technology, Singapore, Singapore, [2]Centre for OptoElectronics and Biophotonics, School of Electrical and Electronic Engineering, Nanyang Technological University, Singapore, Singapore, [3]Adaptive Robotics and Mechatronics Group, Singapore Institute of Manufacturing Technology, Singapore, Singapore

We successfully demonstrate the generation of an all-solid-state deep-ultraviolet (DUV) laser at 206 nm through the fifth (4 + 1)-harmonic generation using a 197-W, 10-kHz, 1.2-ps, 1,030-nm Yb:YAG laser. The DUV laser delivers 180 μJ–582 fs pulses with a peak power of 291 MW, which, to the best of our knowledge, is the highest peak power at 206 nm ever produced by all-solid-state kHz DUV laser sources driven at 1 μm wavelength. This corresponds to one order of magnitude improvement from early state-of-the-art record reported in the literature.

KEYWORDS

deep-ultraviolet, all-solid-state laser, sum frequency generation, 206 nm, sub-picosecond DUV laser, high-power ultrafast lasers

1 Introduction

High-power deep-ultraviolet (DUV) lasers have been widely applied in material processing and scientific studies such as online detection of wafer surface defects, laser drilling, and laser machining of wide bandgap materials [1–3]. In the past decades, excimer lasers have been the workhorse solutions for high-power DUV generation [4]. However, their repetition rates and pulse durations are limited to a few kilohertz and nanoseconds. Furthermore, the poor beam quality and stability, as well as the complex and poisonous maintenance process, make excimer lasers an unsuitable choice in many applications. An all-solid-state laser that uses frequency up conversions from an infrared pump laser is an alternative solution in the DUV region [5–8]. In recent years, significant performance improvements in average power, peak power, and conversion efficiencies of all-solid-state ultrafast DUV laser sources have been reported [9–11]. All-solid-state DUV lasers are put to work in many important scientific and industrial applications such as ultrafast spectroscopy [12], seeding free-electron lasers [13], cold ablation micromachining [14], Z-pinch and laser-produced plasma diagnostics [15], and soft X-ray generation through high harmonic generation in multiply ionized plasmas [16]. Chu et al. developed a 1.37-W DUV laser at 213 nm through sum frequency generation of 532 and 355 nm beams based on a “2 + 3” scheme [17]. High-efficiency fifth-harmonic generation at 211 nm was achieved by cooling the ammonium dihydrogen phosphate (ADP) crystal in a two-chamber cryostat to 200 K [18]. The peak power of DUV lasers in most of the previous developments is limited to a moderate level that sits below a few MW. The fast advances in Yb:YAG laser technology provide a more powerful pump source and make further raising of the DUV laser peak power ceiling possible. However, the peak power scale-up of all-solid-state DUV lasers is not trivial. The large group phase velocity mismatch between the Yb:YAG laser and DUV laser makes the walk-off length extremely short. It limits the effective interaction length for efficient frequency up conversion. The high DUV photon energy makes both linear and non-linear absorption increase quickly with harmonic order. The DUV pulse with high

peak power also induces strong non-linear effects, such as two-photon absorption (TPA) and self-phase modulation (SPM), which lead to high power loss or a destruction of phase-matching conditions. The Kerr-lens effect is also common at high power levels. It is possible to generate filamentation in the crystals and other elements in the optical path, which limits the energy conversion efficiency. To date, the maximum peak power at 206 nm has been reported in the literature and is 12.5 MW [11]. In this paper, we report a 206-nm, 10-kHz, sub-picosecond all-solid-state DUV laser that delivers 180 μJ–582 fs pulses with peak power up to 291 MW, which is one order higher than the previous state-of-the-art record. The DUV laser is generated through fifth (4 + 1)-harmonic generation from a 1.2-ps, 1,030-nm Yb:YAG laser with the same repetition rate and average power of 197 W. We chose β-BaB_2O_4 (BBO) crystals for both fourth-harmonic and final sum frequency generation in the UV region. The high non-linear coefficient of BBO allows us to minimize crystal thickness to avoid the temporal walk-off and undesired non-linear absorption of UV radiation, which is the dominant effect in high peak power DUV laser experiments.

2 Experiment setup

Figure 1 shows a schematic diagram of the experimental setup. Our experimental setup starts from a commercial high power Yb:YAG 1030-nm chirped-pulse amplification (CPA) laser system from InnoSlab amplification technology (AMPHOS 300). The pump laser is able to generate 1,030-nm, 1.2-ps, 20-mJ pulses at 10 kHz with a maximum average power of 220 W [10]. The 1,030-nm pump beam is collimated in advance. A half-wave plate (HWP) and a thin-film polarizer (TFP) are used to precisely control the pump laser power injection to the following stages of the system. A pair of lenses is used to adjust the pump beam size to approximately 9 mm in $1/e^2$ diameter. Lithium triborate (LBO) is chosen for the first second-harmonic generation (2HG) due to its largest damage threshold amongst commercial non-linear crystals [9]. LBO has dimensions of 20 mm × 20 mm × 5 mm, is cut at θ = 90° and φ = 0°, and has a non-critical phase-matching temperature of 190 °C for 1,030 nm and 515 nm. Antireflection (AR) coatings for 1,030 nm and 515 nm are applied on both the entrance and exit surfaces of LBO. We use an electrical oven to maintain a constant LBO temperature. However, a slight phase-match condition drift is observed in the experiment when the pump power rises from zero to maximum. It can be attributed to the limited heating efficiency of the heater, which is only able to attach to the edge of the LBO crystal. The relatively large cross-section size of the crystal makes its center temperature slightly lower than its edge temperature. When the pump laser power increases, the crystal is heated up and the variation in the average temperature and its distribution over the LBO crystal result in a modification of the phase-matching condition. We mount LBO and the oven on a rotational stage and precisely adjust its orientation to compensate for the drift of the phase-matching condition while ramping up the pump laser power. The final oven temperature target is set to 199 °C. Behind LBO, a dichroic mirror is used to remove the residual 1,030-nm pump. For fourth-harmonic generation (4HG), a 515-nm beam is injected into a β-BaB_2O_4 crystal (BBO1) with the dimension of 20 mm × 20 mm × .4 mm and cut at θ = 50° and φ = 0° for type-I phase-matching for second-harmonic generation at 258 nm. BBO is chosen for 4HG due to its high non-linear coefficient, low group velocity dispersion, high optical quality, and non-hygroscopic nature [19]. In our early work, the BBO1 crystal thickness was limited to .4 mm resulting in a maximum energy conversation efficiency and saturation due to non-linear effects such as two-photon absorption (TPA) and self-phase modulation (SPM) [10]. BBO1 has AR coatings for 515 nm and 258 nm on both the entrance and exit surfaces, respectively. The generated 258-nm laser is reflected by using a UV dichromatic mirror (UDM1) to remove the undepleted 515-nm laser. A 258-nm laser is recombined with the residual 1,030 nm power at a second UV dichromatic mirror (UDM2) and injected into a second β-BaB_2O_4 crystal (BBO2) for sum frequency generation. BBO2 has a dimension of 20 mm × 20 mm × .2 mm and is cut at θ = 54.2° and φ = 0° for type-I sum frequency generation of 1030 nm and 258 nm. A delay line and a half waveplate at 1,030 nm (HWP3) are used to

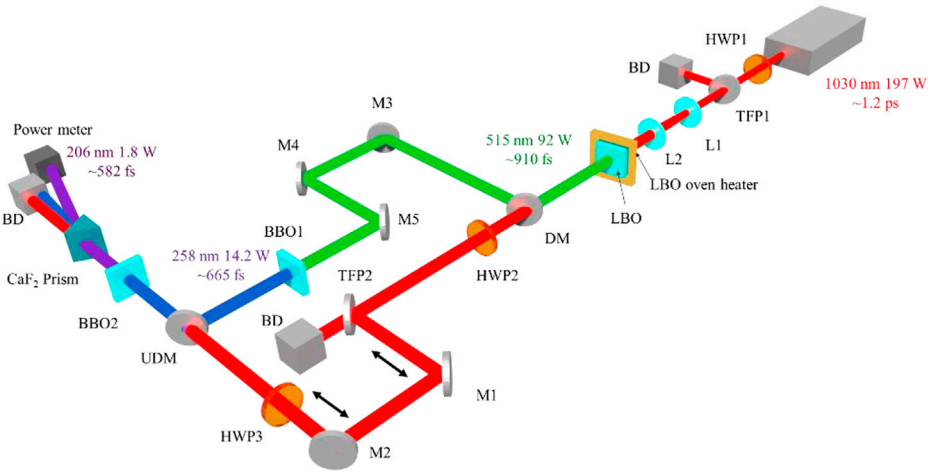

FIGURE 1
Schematic representation of the high-power, sub-ps, all-solid-state DUV laser. HWP, half waveplate; TFP, thin-film polarizer; BD, beam damper; L1–L2, lens; DM, dichroic mirror at 515 nm and 1,030 nm, UDM: UV dichroic mirror at 258 nm and 1,030 nm; M1–M2, 1-μm mirrors; M3–M5, 515-nm mirrors; HWP1–HWP3: half waveplate at 1,030 nm. LBO: lithium triborate; BBO1–BBO2: β-BaB_2O_4.

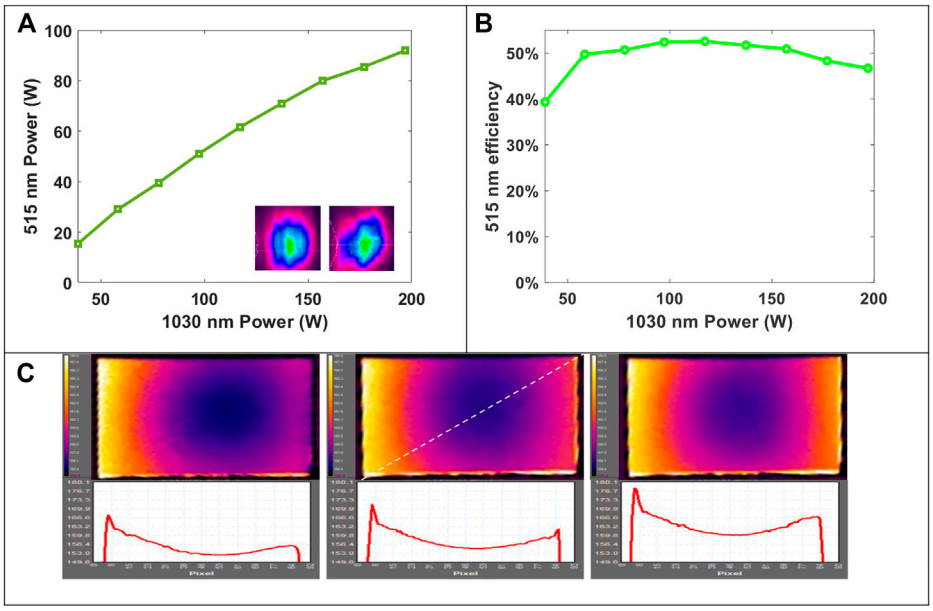

FIGURE 2
Laser average power **(A)** and conversion efficiency at 515 nm **(B)** *versus* the 1-um pump laser average power. Inset shows the 1,030-nm (left) and 515-nm (right) beam profiles (not-to-scale). **(C)** Temperature distribution of the LBO crystal entrance surface at (left to right) 0%, 50%, and 100% pump power. Inset under each photograph: temperature profile along a diagonal line; temperature color range: 150°C–180°C.

compensate for the temporal walk-off and angular walk-off between signal and pump beams that can potentially accumulate in the early stages. Another half-wave plate (HWP2) and a thin-film polarizer (TFP2) are used to control the power of 1,030-nm lasers participating in the final sum frequency generation. The surfaces of BBO2 in 5HG are all uncoated to avoid damage caused by deep-ultraviolet photons. The generated laser beams are spatially separated using a CaF_2 equilateral dispersive prism (Thorlabs) for characterization.

3 Experimental results and discussion

Throughout the paper, the energy conversion efficiencies are defined as the ratio of the output energy at a high harmonic or sum frequency, 2 ω, 4 ω, and 5 ω after the crystal to the input energy at the pump or the corresponding low-order harmonic wavelength, 1 ω, 2 ω, and 4 ω before the same crystal. The LBO crystal is hosted in an electrical oven and heated up slowly in advance. Once the oven temperature is stable at 199 °C, the 1030-nm pump laser is injected into the LBO crystal for second-harmonic generation. To avoid crystal damage, the 1,030-nm pump laser power is ramped up slowly with a step of 10%. The $1/e^2$ beam diameter of the pump laser is maintained at 11.5 mm (long axis) with a maximum power and laser intensity of 197 W and 31.6 GW/cm^2, respectively. The pump laser repetition rate is 10 kHz. Figures 2A, B show a 515-nm power and energy conversion efficiency. We notice that due to the overall crystal temperature variation, there is a monodirectional drift of the phase-matching condition with the rise in pump laser power. Hence, the pump laser incident angle needs to be adjusted slightly at every power level to optimize the 2HG efficiency. Figure 2C shows the temperature profile of the LBO crystal entrance surface that is recorded by using a thermal camera (FLIR T620). Our LBO crystal has a relatively large 15 mm × 15 mm lateral dimension compared with its 5 mm thickness. The oven heater and thermal sensor are only able to be attached to the flank surfaces of the crystal. The heat loss in the propagation path from the edge to the lateral center of the crystal cannot be neglected. Without the pump laser, we find the LBO crystal surface temperature is about 152 ~ 169℃ with a gradient of $\Delta T = T_{edge} - T_{center} = 17$℃. We expected that the pump laser absorption would reduce the thermal gradient ΔT and flatten the surface temperature profile. However, when the 1,030-nm pump laser power rose from 0 to 197 W, the LBO temperature increased at an average of 7.5℃ quite homogenously over the whole entrance surface 159 ~ 177℃. There is very minor variation in the temperature profile shape. At full pump power, the temperature gradient is $\Delta T = 18$℃, which is slightly larger than the case without the pump laser. It can be explained by noting that the heat and 2HG generation are proportional to the pump laser intensity and its square, respectively. Therefore, the center of the pump beam, where it has higher intensity, has more efficient 2HG and suppresses the heat generation by linear absorption of the pump laser. Obviously, the oven heating, rather than the pump laser absorption, dominates not only the mean value but also the spatial profile of LBO temperature. We calculated the optimal phase-matching angle using SNLO and found that the overall temperature variation leads to $\Delta\varphi = 0.8°$, which matches well with the observed 1° variation on the optimal incidental angle in experiments. The maximum output power at 515 nm is 92 W when the pump laser power rises to 197 W. Figure 2A inset shows the beam profile of the 515-nm laser after the LBO crystal. The green laser slightly diverges with a long axis $1/e^2$ beam diameter of 8.5 mm and a peak intensity of 35.6 GW/cm^2. Compared with the results reported in [10], the drop in pump laser power not only reduces the 2HG beam diameter and intensity but also suppresses the self-focusing effect and changes the divergence

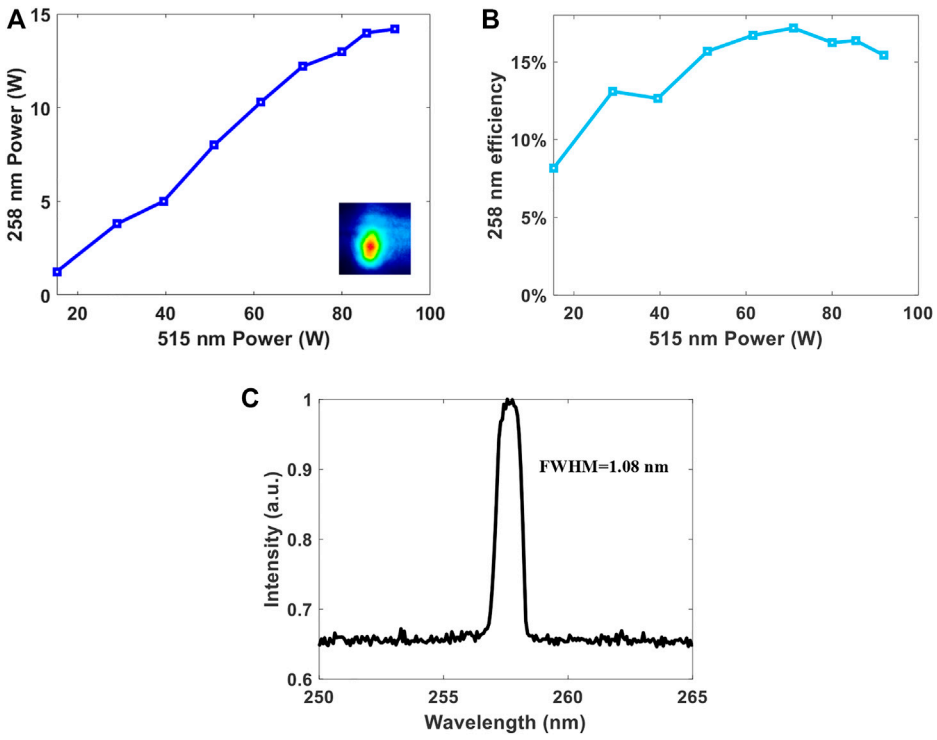

FIGURE 3
Average power **(A)** and conversion efficiency at 258 nm **(B)** *versus* the average pump laser power at 515 nm. Inset shows the 258-nm beam profile. **(C)** Spectrum of the 258-nm laser with a FWHM of 1.08 nm.

of the green laser beam. Saturation of the energy conversion efficiency is observed when the 1,030-nm pump power approaches 117 W, which matches well with the similar observation at 110 W reported in [10]. These results prove the reliable and repeatable construction of the longitudinal temperature gradient (LTG) in the LBO crystal, which is believed to be the major reason for the energy conversion efficiency decreasing in previous work [20].

We chose β-BaB_2O_4 (BBO) crystals for both 4HG and 5HG due to their high non-linear coefficient (~2.6 p.m./V) [19]. It allows us to use a shorter crystal length to minimize undesired reabsorption of UV radiation through non-linear effects such as two-photon absorption (TPA) or self-phase modulation (SPM), which are dominant effects observed in our experiments. Figures 3A, B show the power and energy conversion efficiency at 258 nm *versus* the input laser power at 515 nm. Weak saturation on the conversion efficiency is observed when the 515-nm power is beyond 71 W, corresponding to an intensity of 2.75 GW/cm^2. BBO1 has a thickness of .4 mm, which is very thin for LTG construction and is also shorter than the 1-mm walk-off length between 515 nm and 258 nm. The observed saturation can only be attributed to TPA of 258 nm in the crystal. Figure 3A inset picture shows the output laser of 258 nm has an elliptical beam profile with a long axis 1/e^2 beam diameter of 6.6 mm. The maximum average power at 258 nm obtained in the experiment is 14.2 W, which corresponds to a power intensity of 12.5 GW/cm^2. Figure 3C shows the measured spectrum of the 258-nm beam, which has an FWHM bandwidth of 1.08 nm. The limited power and more diverged beam profile at 515 nm cause an overall 4HG efficiency that is lower than our early experiment [10]. However, using the diverged beam helps avoid damaging other optic elements in the subsequent 5HG optical path. It helps to avoid self-focusing effect and the generation of filamentation in following optics elments such as CaF_2 prism before the power meter especially well.

Finally, the generated 258-nm beam is combined with the residual 1,030-nm beam at BBO2 for 5HG at 206 nm through sum frequency generation. To identify the optimal BBO crystal thickness, we test three BBO crystals with the thicknesses of .1 mm, .2 mm, and .4 mm and apertures of 20 mm × 20 mm in experiments. Figure 4A shows the dependence of the average power at 206 nm on the crystal thickness at different 1,030-nm pump laser power levels. The walk-off length between 1,030 nm and 206 nm is about .3 mm. Therefore, the BBO crystal with .1 mm thickness is not able to induce significant temporal walk-off and TPA at 258 nm or 206 nm. The output 206-nm power monochromatically increases with 1,030-nm pump power without observing a strong saturation phenomenon. However, the energy conversion efficiency is very limited, and the maximum output power at 206 nm is about .8 W. In the case of BBO crystal with .2 mm, a much higher energy conversion efficiency is observed, especially at low or moderate 1,030 nm pump power levels. The maximum output power at 206 nm is 1.8 W, which is slightly above two times of that obtained with a .1-mm thick crystal. A weak saturation effect appears when pump power at 1,030 nm is beyond 117 W, which corresponds to 61.6 W at 515 nm and 10.3 W at 258 nm (~9.05 GW/cm^2 at BBO2). We believe it is an amplification of LTG-induced LBO gain saturation in the early stage, as shown in Figure 2. TPA of 258 nm in Figure 3 is also observed at a slightly higher 1,030-nm pump power of 137 W, which corresponds to 71 W at 515 nm and 12.2 W at 258 nm (~10.7 GW/cm^2 at BBO2). When BBO crystal thickness is increased to .4 mm, which is beyond the walk-off

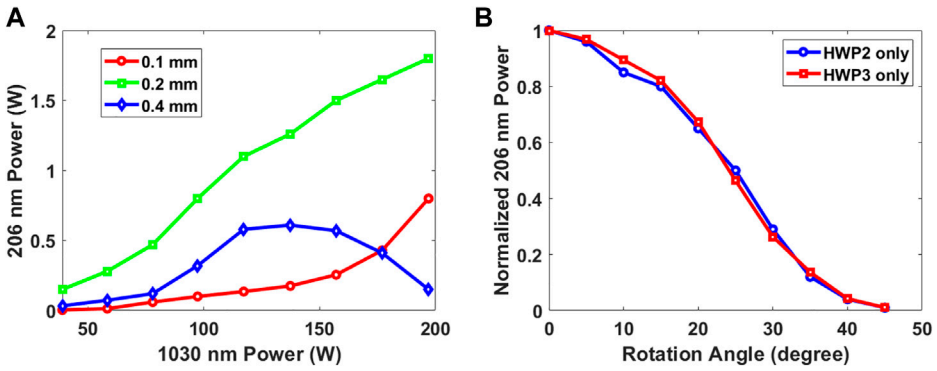

FIGURE 4
(A) Power at 206 nm *versus* the 1,030-nm pump laser power for different thicknesses of BBO2. **(B)** Power variation at 206 nm with respect to the power (HWP2 only) and polarization (HWP3 only) of the 1,030-nm laser.

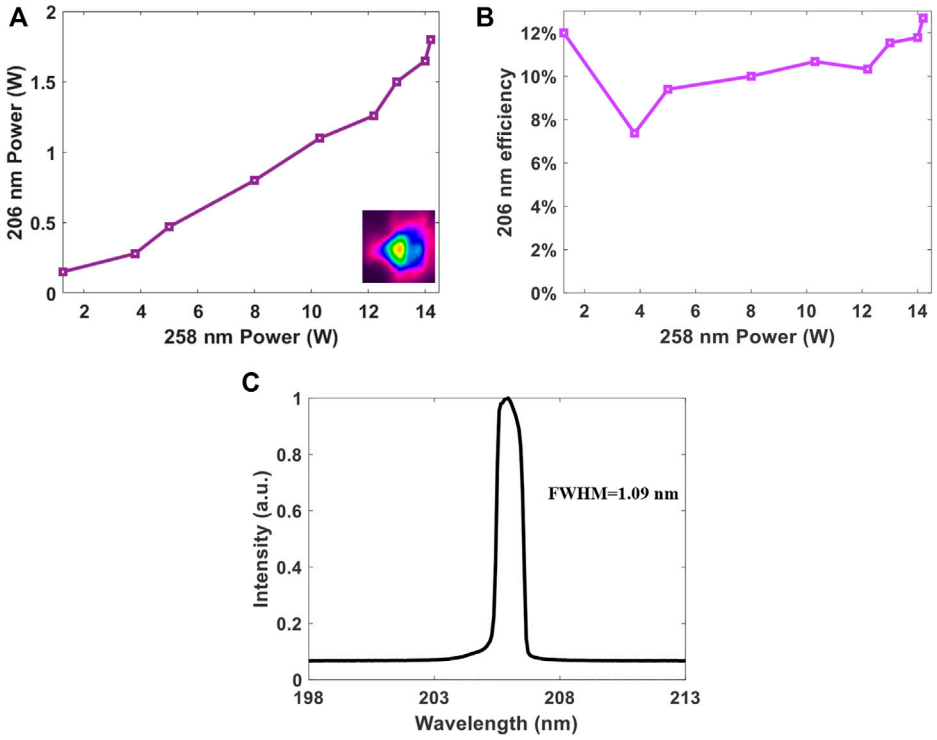

FIGURE 5
Average power **(A)** and conversion efficiency at 206 nm **(B)** *versus* the average pump laser power at 258 nm. The inset in **(A)** is the beam profile of the output 206-nm beam. **(C)** Spectrum of the 206-nm laser with a FWHM of 1.09 nm.

length, between 1,030 nm and 206 nm, significant energy conversion efficiency decreases are observed at several stages of pump laser power. First of all, when the 1,030-nm pump power is below 78 W, the power generated at 206 nm from a .4-mm thick BBO is less than 20% of that from a .2-mm thick BBO. Second, when the 1,030-nm power is in the range between 78 W and 117 W, higher 258-nm pump power benefits more to sum frequency generation than TPA or other non-linear absorptions. Power generated at 206 nm from the .4-mm thick BBO rose to about 50% of that from the .2-mm thick BBO. Third, when pump power at 1,030 nm is beyond 117 W, corresponding to more than 12 W (>10 GW/cm^2), power at 258 nm is applied to BBO2 and the output 206-nm power quickly drops to zero. Linear absorption coefficients of the BBO at 206 nm, 258 nm, and 1,030 nm are .0866 cm^{-1}, .00836 cm^{-1}, and .00004 cm^{-1}, respectively [21]. With just a .2 mm increase on crystal thickness, it is impossible to generate up to 80% power loss observed in the experiment as both pump lasers used in our sum frequency generation have high peak intensities of 15.6 GW/cm^2 at 1,030 nm and 12.5 GW/cm^2 at 258 nm.

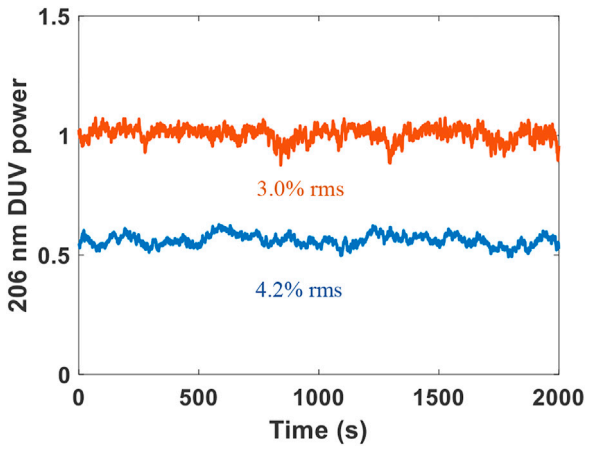

FIGURE 6
DUV power stability of 206 nm at .5 W and 1 W average power for a 2,000-s time window.

It likely hints that there exists a very strong TPA or even a high-order non-linear absorption condition in our experiments. Figure 4B shows a 206-nm power variation with respect to power and polarization of a 1,030-nm laser that participates in the sum frequency generation on BBO2. They are implemented by rotating the two half waveplates HWP2 and HWP3 separately. Polarization tuning shows almost the same influence on the sum frequency generation as that seen through power tuning at 1,030 nm. It means that the non-linear absorption, which depends on the total power, mainly occurs at 258 nm and 206 nm but not at 1,030 nm in BBO2. However, non-linear absorption alone cannot explain the variation of power at 206 nm with respect to the pump power. We suspect that destructive interference induced by the pump power-dependent phase modulation mechanism also plays an important role in our experiment. The possible reasons for the suspected phase modulation mechanism include spatial-temporal wavefront modulation, accumulated pulse chirps, and non-linear refractive index modulation induced by the high pump laser intensity. Identification of the exact physics behind it can be explored in the future, which is beyond the scope of this paper.

Obviously, the BBO crystal with a thickness of .2 mm is the optimal choice for sum frequency generation. Figures 5A, B show the power and energy conversion efficiency at 206 nm *versus* the input laser power at 258 nm with a .2-mm thick BBO2. Figure 5A inset picture shows the laser beam profile at 206 nm. The maximum pump power at 258 nm and 1,030 nm that participates in the sum frequency generation is 14.2 W (12.5 GW/cm^2) and 97 W (15.6 GW/cm^2), respectively. The output at 206 nm has a long axis 1/e^2 beam diameter of 6.1 mm with a maximum power of 1.8 W. Figure 5C shows the measured spectrum of the 206-nm beam, which has an FWHM bandwidth of 1.09 nm and is able to support a 57.3-fs Fourier transform limited (FTL) pulse duration. The 206-nm pulse duration is estimated to be ~582 fs by the sum frequency formula $\tau = \tau_1\tau_2/\sqrt{\tau_1^2 + \tau_2^2}$, where $\tau_1 = 1.2\ ps$ and $\tau_2 = 665\ fs$ are 1,030 nm pulse duration and 258 nm pulse duration measured in our previous paper [10]. Based on the calculated pulse duration, the peak power of the 206-nm laser is estimated to be as high as 291 MW, which is the highest peak power for a 10-kHz rate, all-solid-state DUV source at 206 nm driven by a 1-μm pump laser at the time of writing.

Finally, the operation stability is investigated at .5 W and 1 W average power outputs at 206 nm, as shown in Figure 6. In both cases, the data are recorded about 10 min later after the injection of the pump laser and after the output at 206 nm had become stable. Some particle trapping on the optic surface was expected. Moreover, no surface degradation and bulk optical degradation of BBO crystal are observed after the test.

4 Conclusion

We have demonstrated a 206-nm DUV laser through fifth (4 + 1)-harmonic generation of a 1,030-nm, 1.2-ps, 10-kHz Yb:YAG solid-state laser using LBO, BBO, and BBO as 2HG, 4HG, and 5HG crystals, respectively. We obtain a 1.8-W, 180-μJ, 206-nm DUV laser with a pulse duration of ~582 fs, which corresponds to a peak power of 291 MW, which is the highest peak power for a 10-kHz, all-solid-state DUV laser source at 206 nm driven by the Yb:YAG laser at the time of writing. Ultra-thin BBO crystals with high non-linear coefficients are chosen for up-frequency generation at the DUV region. It relaxes the constraints on the maximum pump beam intensity and mitigates the majority of the deleterious effects induced by the strong non-linear response of the crystal on following optic elements in the optical path.

Data availability statement

The original contributions presented in the study are included in the article; further inquiries can be directed to the corresponding author.

Author contributions

QR and HL designed and built the setup. QR measured the data. All authors analyzed the data and contributed to the final manuscript.

Funding

This work was supported by Agency for Science, Technology and Research (A*STAR) 2022 career development fund (C222812005).

Conflict of interest

The authors declare that the research was conducted in the absence of any commercial or financial relationships that could be construed as a potential conflict of interest.

Publisher's note

All claims expressed in this article are solely those of the authors and do not necessarily represent those of their affiliated organizations, or those of the publisher, the editors, and the reviewers. Any product that may be evaluated in this article, or claim that may be made by its manufacturer, is not guaranteed or endorsed by the publisher.

References

1. Okamoto A, Kuniyasu H, Hattori T. Detection of 30–40-nm particles on bulk-silicon and SOI wafers using deep UV laser scattering. *IEEE Trans semiconductor manufacturing* (2006) 19(4):372–80. doi:10.1109/tsm.2006.884600

2. Tan B. Deep micro hole drilling in a silicon substrate using multi-bursts of nanosecond UV laser pulses. *J Micromechanics Microengineering* (2005) 16(1):109–12. doi:10.1088/0960-1317/16/1/015

3. Gow PC, Bannerman RHS, Mennea PL, Holmes C, Gates JC, Smith PGR. Direct UV written integrated planar waveguides using a 213 nm laser. *Opt Express* (2019) 27(20): 29133–8. doi:10.1364/oe.27.029133

4. Basting D, Marowsky G. *Excimer laser technology* (2005). Heidelberg: Springer

5. Yap Y, Inagaki M, Nakajima S, Mori Y, Sasaki T. High-power fourth- and fifth-harmonic generation of a Nd:YAG laser by means of a CsLiB_6O_10. *Opt Lett* (1996) 21(17):1348–50. doi:10.1364/ol.21.001348

6. Sakuma J, Asakawa Y, Imahoko T, Obara M. Generation of all-solid-state, high-power continuous-wave 213-nm light based on sum-frequency mixing in CsLiB_6O_10. *Opt Lett* (2004) 29(10):1096–8. doi:10.1364/ol.29.001096

7. Chen G, Zou H, He X, Shen Y, Liu Q. Fourth harmonic generation based on miniaturized tunable bow-tie resonators. *Opt Laser Tech* (2019) 114:44–8. doi:10.1016/j.optlastec.2019.01.002

8. Begishev I, Bromage J, Yang ST, Datte PS, Patankar S, Zuegel JD. Record fifth-harmonic-generation efficiency producing 211 nm, joule-level pulses using cesium lithium borate. *Opt Lett* (2018) 43(11):2462–5. doi:10.1364/ol.43.002462

9. Chang C-L, Krogen P, Liang H, Stein GJ, Moses J, Lai CJ, et al. Multi-mJ, kHz, ps deep-ultraviolet source. *Opt Lett* (2015) 40(4):665–8. doi:10.1364/ol.40.000665

10. Liu K, Li H, Qu S, Liang H, Wang QJ, Zhang Y. 20 W, 2 mJ, sub-ps, 258 nm all-solid-state deep-ultraviolet laser with up to 3 GW peak power. *Opt Express* (2020) 28(12): 18360–7. doi:10.1364/oe.395948

11. Willenberg B, Brunner F, Phillips CR, Keller U. High-power picosecond deep-UV source via group velocity matched frequency conversion. *Optica* (2020) 7(5):485–91. doi:10.1364/optica.386257

12. Kobayashi T, Kida Y. Ultrafast spectroscopy with sub-10 fs deep-ultraviolet pulses. *Phys Chem Chem Phys* (2012) 14(18):6200–10. doi:10.1039/c2cp23649d

13. Allaria E, Castronovo D, Cinquegrana P, Craievich P, Dal Forno M, Danailov MB, et al. Two-stage seeded soft-X-ray free-electron laser. *Nat Photon* (2013) 7(11):913–8. doi:10.1038/nphoton.2013.277

14. Račiukaitis G, Brikas M, Gedvilas M, Darcianovas G. Patterning of ITO layer on glass with high repetition rate picosecond lasers. *J Laser Micro/Nanoengineering* (2007) 2(1): 1–6. doi:10.2961/jlmn.2007.01.0001

15. Ivanov V, Anderson A, Begishev I. Four-color laser diagnostics for Z-pinch and laser-produced plasma. *Appl Opt* (2016) 55(3):498–501. doi:10.1364/ao.55.000498

16. Popmintchev D, Hernandez-Garcia C, Dollar F, Mancuso C, Perez-Hernandez JA, Chen MC, et al. Ultraviolet surprise: Efficient soft x-ray high-harmonic generation in multiply ionized plasmas. *Science* (2015) 350(6265):1225–31. doi:10.1126/science.aac9755

17. Chu Y, Zhang X, Chen B, Wang J, Yang J, Jiang R, et al. Picosecond high-power 213-nm deep-ultraviolet laser generation using β-BaB2O4 crystal. *Opt Laser Tech* (2021) 134: 106657. doi:10.1016/j.optlastec.2020.106657

18. Begishev I, Brent G, Carey S, Chapman R, Kulagin IA, Romanofsky MH, et al. High-efficiency, fifth-harmonic generation of a joule-level neodymium laser in a large-aperture ammonium dihydrogen phosphate crystal. *Opt Express* (2021) 29(2):1879–89. doi:10.1364/oe.415691

19. Nikogosyan DN. *Nonlinear optical crystals: A complete survey*. New York: Springer Science & Business Media (2006).

20. Wu S, Blake GA, Sun S, Ling J. A multicrystal harmonic generator that compensates for thermally induced phase mismatch. *Opt Commun* (2000) 173(1-6):371–6. doi:10.1016/s0030-4018(99)00580-5

21. Tamošauskas G, Beresnevicius G, Gadonas D, Dubietis A. Transmittance and phase matching of BBO crystal in the 3–5 μm range and its application for the characterization of mid-infrared laser pulses. *Opt Mater Express* (2018) 8:1410–8. doi:10.1364/ome.8.001410